# Specific features of differential motions in the DIMM

V. Kornilov, B. Safonov

May 28, 2010

## 1 Introduction

Differential image motion monitor DIMM widely used in studies of optical turbulence, is destined to measure the integrated effect of the Earth's atmosphere on the image quality. The advantages of this tool are obvious: a simple and reliable device for longstanding and field studies, measurements are easily interpreted on the basis of the theory of light propagation through turbulent media, the result is directly linked to the main astroclimatic characteristics — image quality, i.e. seeing.

However, there are several effects that produce the systematic and random errors in measurements with the DIMM instrument. Although these effects were discussed many times, acceptable unambiguity and certainty in their estimate has not been achieved. This paper presents the results of additional analysis and impact assessments of the following effects on real measurements:

1. The effect of the propogation of the distorted wave (discard of the near-field approximation).
2. The effect of the width of the spectral band of radiation (the polychromatic effect).
3. The effect of finite exposure. Method of correlation to account for this effect.
4. The influence of the duration of measurement. Evaluation of low-frequency input of differential motion.

The preparation for the processing of data obtained with MASS/DIMM instrument in 2007 - 2009 at Mt. Shatdzhatmaz, initiated the development of a practical method of accounting for these effects in scope of joint processing of MASS and DIMM measurements.

In the first two sections the basics of the theory are presented, which describes the effect of differential image motion in the approximation of small perturbations — a situation which, as a rule, implemented in typical conditions of astronomical observations. This basis then are used for the case with the wave propagation and for introducing of the concept of DIMM weighting function for later practical use. In section 5 weighting function for the case of polychromatic light is calculated.

## 2 The spatial spectrum of differential motions

Expressions for the spatial spectrum of differential motions are given in the classical works of Fried [1] and Martin [2]. In the work of Martin, they are obtained by gradual spatial filtering

of the power spectrum of phase perturbations in the assumption of Kolmogorov's model of the optical turbulence (OT).

, $F_\phi(f_x, f_y)$ $J = C_n^2 \Delta h$ : It is known that the spectral power density of phase fluctuations $F_\phi(f_x, f_y)$ proportional to the intensity of optical turbulence $J = C_n^2 \Delta h$ in the homogeneous and isotropic layer:

$$F_\phi(f_x, f_y) = F_\phi(f) = 0.0229 r_0^{-5/3} f^{-11/3} = 0.0229 \cdot 0.423 \left(\frac{2\pi}{\lambda}\right)^2 J\, f^{-11/3}, \tag{1}$$

where $f = (f_x^2 + f_y^2)^{1/2}$ — modulus of spatial frequency, $f_x$ and $f_y$ — spatial frequency components, and $r_0$ — Fried parameter. For practical purposes, is preferable to consider the $J$, since this value is used to describe the vertical profile of the OT.

The expression for the power spectrum of differential motion will depend on what is meant under the center of the image. This is important because the distorted wave front is not flat within the used aperture and image is not diffraction nor axis-symmetric even. Usually it is a center of gravity of the image (g-tilt) [2], or the normal to approximating the wave front plane (z-tilt) [3]. The difference between the two approaches is analyzed in the paper [4].

The spatial spectrum of the differential motion in the sense of the center of gravity of the image, built objective with an aperture of $D$ seems as follows [2]:

$$F_a^g(f_x, f_y) = \left(\frac{\lambda}{2\pi}\right)^2 (2\pi(f_x \cos\theta + f_y \sin\theta))^2 \left[\frac{2J_1(\pi D f)}{\pi D f}\right]^2 F_\phi(f_x, f_y), \tag{2}$$

where $\theta$ — the angle between the x axis and the direction in which the motion is measured. For further conveniently, the x-axis is directed along the direction of the wind.

The spectral density $F_d(f_x, f_y)$ of the differential motion, measured in the DIMM, is obtained by multiplying the $F_a$ at the spectral filter corresponding two apertures placed at a separation $B$ at an angle $\theta - \psi$ from axis x:

$$F_d(f_x, f_y) = [2\sin(\pi B(f_x \cos(\theta - \psi) + f_y \sin(\theta - \psi)))]^2 F_a(f_x, f_y) \tag{3}$$

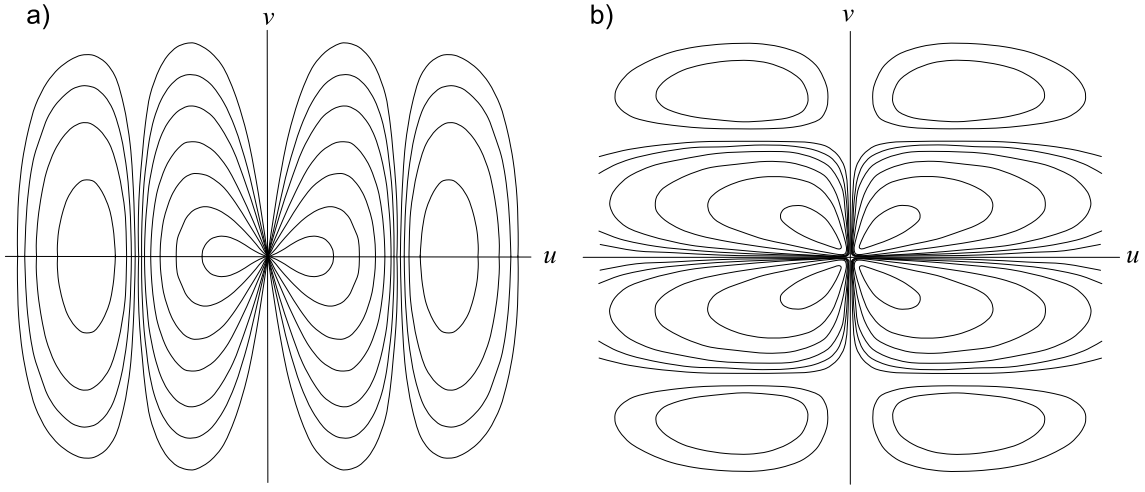


Figure 1: Contour representation of the spectral power density of differential motion in a) longitudinal and b) transversal directions. DIMM apertures are directed along the axis u. Contour curves are plotted on a logarithmic scale in increments of 0.5.

The values of $\psi = 0$ corresponding to the longitudinal motion (along the base of the instrument) and $\psi = \pi/2$ corresponding to the transversal motion, have practical meaning. In Fig. 1 two-dimensional contour image of the spectral power density for these cases are shown. In the picture, the DIMM base is directed along the axis of x, if to rotate the base, the picture will be rotated with it. Note the principal difference in the form of the spatial spectrum for the longitudinal and transversal cases — first has a dipole structure, and the second has a quadrupole one. In both cases, the power density when $|f| = 0$ is zero.

Note that after substitution of (1) in (2) the final expression for the spectral density will not depend on wavelength $\lambda$. The motion variance, by definition, expressed in terms of their power spectrum as follows:

$$\sigma_d^2 = \iint_{-\infty}^{+\infty} F_d(f_x, f_y)\,\mathrm{d}f_x\,\mathrm{d}f_y, \tag{4}$$

Really, substituting here ((3) and integrating, we obtain the necessary practical expression relating the measured differential motion and turbulence intensity $J$ of the layer. In the approximation of small perturbations can be further integrated expression 4 along the line of sight and get a well-known formula from [5].

Recall that the expression (2) is obtained for the case of near-field approximation, that is, excluding the effect of propagation of the distorted light wave.

Similarly, one can find the appropriate expression for the differential motion power in the sense of z-tilt, using the lightly modified expression from the work [4]

$$F_a^z(f_x, f_y) = \left(\frac{\lambda}{2\pi}\right)^2 (2\pi(f_x\cos\theta + f_y\sin\theta))^2 \left[\frac{8J_2(\pi Df)}{(\pi Df)^2}\right]^2 F_\phi(f_x, f_y) \tag{5}$$

The spectral density in the sense of z-tilt differs from $F_a^g(f_x, f_y)$ only with the aperture filter. This filter is somewhat wider than the g-tilt aperture filter, although its transmission decreases rapidly at the high frequencies

## 3 The temporal spectra of differential motion

The temporal spectra of the differential motion have greater practical interest than the spatial spectra, since the real device registers the image motion from frame to frame, obtained at different times.

At first, we consider an isolated turbulent layer moving with constant velocity $w$. The subsequent transformation of the spatial spectrum to the temporal one is based on Taylor's hypothesis of the frozen turbulence [7], i.e. on the assumption that the phase distortions vary significantly slower than the $D/w$. For this case, the temporal power spectrum of differential motion is given by [2]:

$$F_d(\nu) = \frac{2}{w}\int_0^\infty \mathrm{d}f_y\, F_d(\frac{\nu}{w}, f_y) \tag{6}$$

Recall that the x-axis is directed along the wind. Due to the fact that the spatial spectrum does not possess central symmetry, the temporal spectra will be different for different directions of the DIMM base. Normalized spectra $F_d(\nu)$ calculated for 4 directions of wind are presented in Fig. 2.

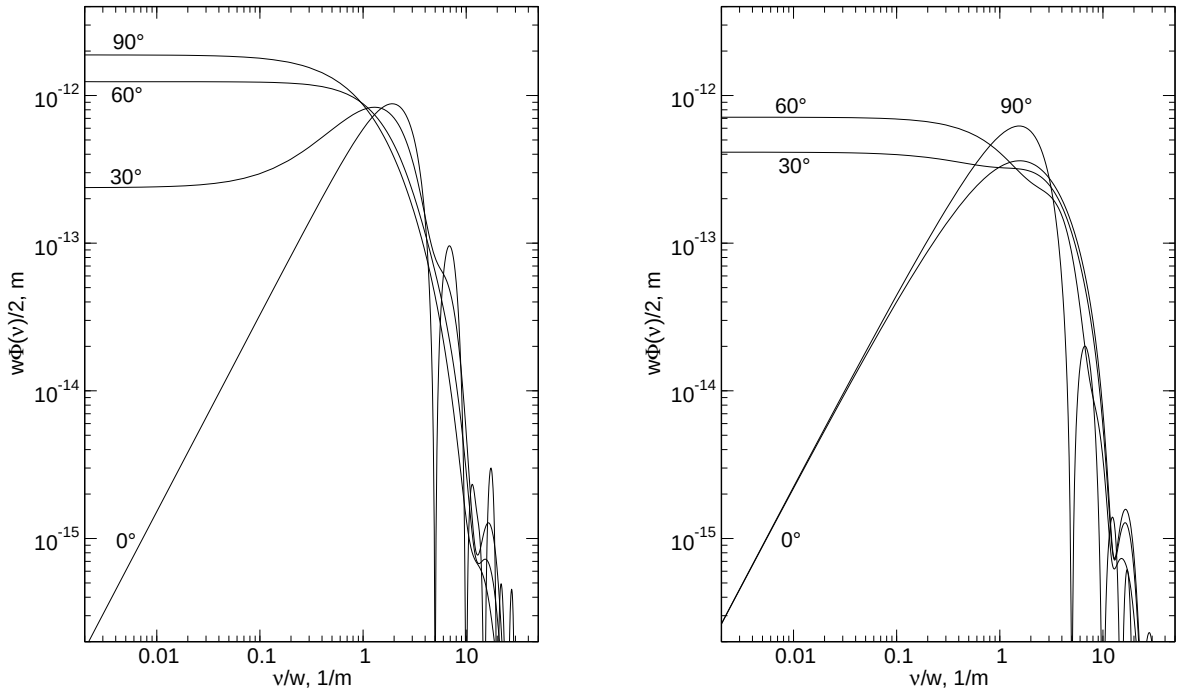


Figure 2: The temporal spectra of differential motion for different wind directions relative to the base. The spectra are normalized at wind speed. The curves are calculated for $D = 0.09$ m, $B = 0.2$ m and $r_0 = 0.1$ m. The spectra for the longitudinal motion are presented on left, for the transversal on right

It is clear that in a real situation the wind fluctuates greatly on speed and direction. Therefore, the final power spectrum will be a complex composition of many individual spectra. First of all smeared quasi-periodic details in the high-frequency, and the spectrum converges to the dependence $\nu^{-1}$. In the low-frequency $\nu \ll w/D$ the spectrum is determined by the slow layer with noticeable turbulence, mainly — by ground layer. Depending on the angle between the wind direction and the DIMM base, the power of differential motion comes or at a constant level or down as power law with exponent 4/3 with the frequency approached to 0.

In our case, separating these domains characteristic frequency is $1-3$ Hz for a typical ground winds. Analysis of the low-frequency region of the spectrum can not be correct, because the use of the "frozen" hypothesis at such times is not always legal.

# 4 Taking account of wave propagation — DIMM weighting functions

The whole theory and practice of determining the seeing $\beta$ from differential motion, measured with DIMM, are built in the approximation of near-field diffraction, ie the case of $D^2 \gg \lambda z$. However, for real devices in real situations, this condition is not always satisfied.

The problem escalated after the appearance of large amounts of measurements with the

MASS/DIMM instrument, when it became clear that there are many cases of dominant high-altitude (8 – 24 km) turbulence. In practice this leads to the fact that the DIMM underestimate the total intensity of the OT, and efforts to calculate the intensity of the surface layer as $J_{DIMM} - J_{MASS}$ results to negative intensities in the surface layer [5, 6, 8].

This problem was noted in many studies, such as [5], and the impact of the effect was assessed in [4, 9]. Nevertheless, no practical steps to correct the underestimation of high OT has not been fulfilled.

Prove that the correction is possible in the terms of the weighting functions (used in the theory MASS [10, 11]), i.e. a dependence of the variance of differential motion $\sigma^2$ on the profile of the turbulence $C_n^2(z)$ may be represented as follows:

$$\sigma^2 = \int_0^\infty C_n^2(z) W(z)\,\mathrm{d}z, \tag{7}$$

To account for the propagation effect of distorted light wave from the layer located at a distance of $z$ is sufficient in the formula (1) for the spectral power density of phase fluctuations add a Fresnel filter $\cos^2(\pi\lambda z f^2)$, as done in [4]:

$$\Delta F_\phi(f, z) = 0.009687 \left(\frac{2\pi}{\lambda}\right)^2 C_n^2(z)\Delta z\, f^{-11/3} \cos^2(\pi\lambda z f^2), \tag{8}$$

Further transformations are based on the fact that in the approximation of weak perturbations the power of phase fluctuations of the wave is the sum of the power spectra of all thin layers, which it crosses [7]:

$$F_\phi(f) = 0.009687 \left(\frac{2\pi}{\lambda}\right)^2 \int_0^\infty C_n^2(z) f^{-11/3} \cos^2(\pi\lambda z f^2)\,\mathrm{d}z. \tag{9}$$

Obviously, since none of the three filters (the gradient, aperture and differential) does not depend on the distance $z$ we can perform integration with respect to the frequency before integration over $z$. Denote the full spectral filter as $\left(\frac{\lambda}{2\pi}\right)^2 \Phi(f_x, f_y)$. Recall that this filter depends on the parameters of the device $D$, $B$ and the motion angle $\psi$. Then the expression for the variance of the differential motion can be written, omitting the subscript $d$, as:

$$\sigma^2 = \int_0^\infty \mathrm{d}z\, C_n^2(z) \times 0.009687 \iint_{-\infty}^{+\infty} \mathrm{d}f_x\,\mathrm{d}f_y\,\Phi(f_x, f_y) f^{-11/3} \cos^2(\pi\lambda z f^2). \tag{10}$$

The inner double integral can be interpreted as altitude weighting function DIMM $W(z)$, depending on the parameters of a particular device as well as MASS weighting functions. The practical application requires to calculate two such functions — $W_l(z)$ for longitudinal and $W_t(z)$ for the transversal motion.

$$W_{l,t}(z) = 0.009687 \iint_{-\infty}^{+\infty} \mathrm{d}f_x\,\mathrm{d}f_y\,\Phi_{l,t}(f_x, f_y) f^{-11/3} \cos^2(\pi\lambda z f^2). \tag{11}$$

Transforming to polar coordinates in expression (11) it can be integrated analytically over the angle $\phi$ [2] and the formula for the weighting function becomes:

$$W_{l,t}^{g,z}(z) = 0.009687 \times 8\pi^3 \int_0^\infty \mathrm{d}f\, I^{g,z}(f) \left[1 - 2\cos^2(\psi) J_0(2\pi f B) + 2\cos(2\psi)\frac{J_1(2\pi f B)}{2\pi f B}\right]. \tag{12}$$

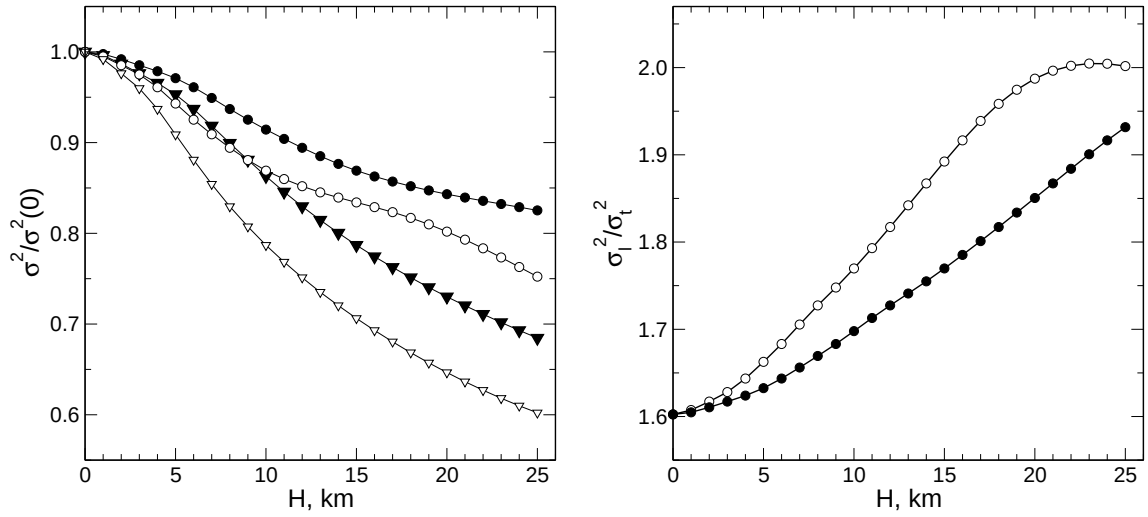


Figure 3: *Left*: normalized to near-field approximation weighting functions DIMM $W(h)/W(0)$ for the case of g-tilt. Circles — the longitudinal motion, triangles — transversal. *Right*: the ratio of longitudinal to transverse variances. Filled symbols — calculation for $\lambda = 500$ nm, the empty — for $\lambda = 750$ nm

Note that the difference in the weighting functions for the cases of g-tilt (2) and the z-tilt (5) is described by the term $I^{g,z}(f)$ depending only on the modulus of frequency:

$$I^g(f) = f^{-2/3}\left[\frac{2J_1(\pi f D)}{\pi f D}\right]^2 \cos^2(\pi\lambda z f^2), \tag{13}$$

$$I^z(f) = f^{-2/3}\left[\frac{8J_2(\pi f D)}{(\pi f D)^2}\right]^2 \cos^2(\pi\lambda z f^2). \tag{14}$$

Given that $\psi = 0$ for the longitudinal motion and $\psi = \pi/2$ for the transversal one, we obtain finally:

$$W_l^{g,z}(z) = 2.403\int_0^\infty \mathrm{d}f\, I^{g,z}(f)\left[1 - 2J_0(2\pi f B) + 2\frac{J_1(2\pi f B)}{2\pi f B}\right] \tag{15}$$

$$W_t^{g,z}(z) = 2.403\int_0^\infty \mathrm{d}f\, I^{g,z}(f)\left[1 - 2\frac{J_1(2\pi f B)}{2\pi f B}\right] \tag{16}$$

Calculation of $W_{l,t}(z)$ can be made by numerical integration, just as in the program *atmos* the set of weighting functions MASS are computed. Note that in contrast to the near-zone approximation, the wavelength dependence of differential motion is appeared and, consequently, the dependence on the spectral composition of radiation. Directly integrate over $\lambda$, as well as in the case of weight functions MASS [12], can not be performed due to the motions in close wavelengths are strongly correlated. However, of the smallness of the effect (it is certainly less than a factor of 0.5) some effective wavelength can be used.

In Fig. 3 the weighting functions are presented, calculated for our instrument and normalized to its value at zero altitude. In fact, the weight functions depend on one parameter — Fresnel

radius $r_F^2 = \lambda z$, so the change in wavelength can easily compensate for changes in altitude. For example, in Fig. 3 weights for $\lambda = 750$ nm are transformed into curves for $\lambda = 500$ nm by scaling to 1.5 times in altitude.

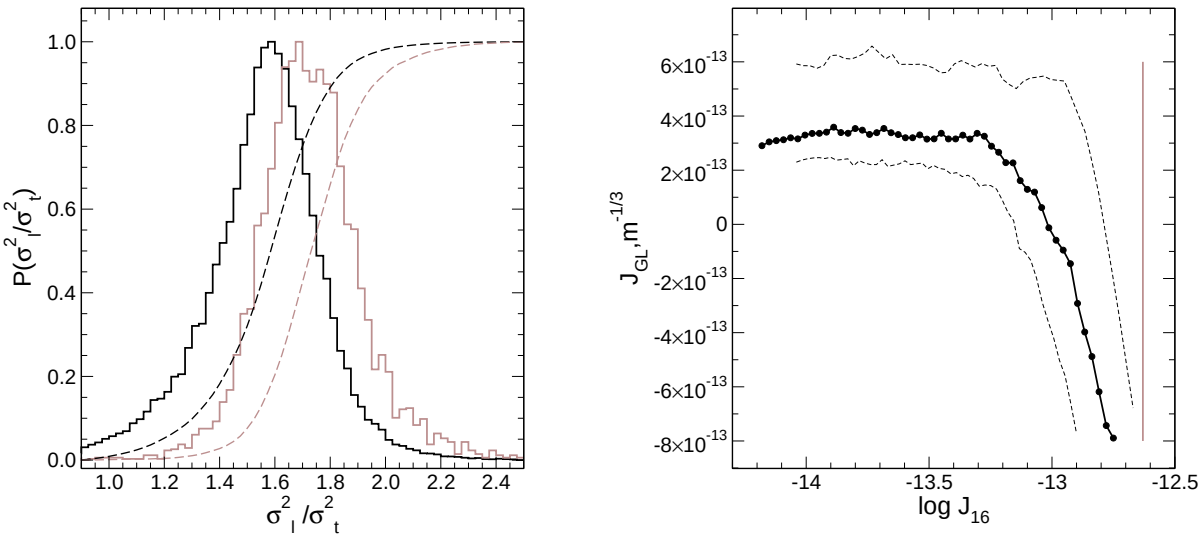


Figure 4: Left: Distributions of the measured ratio $\sigma_l^2/\sigma_t^2$ for "positive" (black) and "negative" (light) graund layer OT $J_{DIMM} - J_{MASS}$. Right: Dependence of medians of graund layer OT on intensity OT in 16 km layer. Dashed lines are 25  75% quartiles. Light vertical line corresponds to OT generating scintillation index 0.3 for A aperture of MASS device

Note the significant difference between the behavior of $W_l(z)$ and $W_t(z)$, resulting from differences in the form of spatial spectra of longitudinal and transverse components of motion (Fig. 1). As a result, the ratio $\sigma_l^2/\sigma_t^2$ varies with the altitude as shown in Fig. 3 on right.

This effect can be observed in practice, if we select the situation with a dominant high turbulence. All results of preprocessing performed in the approximation of the near-zone, were divided into two groups: with positive OT intensity in the ground layer and with negative value of $J_{DIMM} - J_{MASS}$. Effect of high-altitude turbulence is confirmed by the distributions of the observed ratio $\sigma_l^2/\sigma_t^2$ for these two groups, presented on the left in Fig. 4. Median values are 1.58 and 1.73, respectively.

In right part of Fig. 4 the behavior of the median value of $J_{DIMM} - J_{MASS}$ is shown as dependence on the intensity of the 16 km layer $J_{16}$. It is evident that the effect of "negative" ground turbulence is indeed induced by underestimation of high-altitude turbulence. Bend of the medians curve begins long before the scintillation generated 16 km layer reaches saturation, and therefore can not be fully explained by the revaluation of OT with the instrument MASS.

As shown in [4], actually used in the DIMM method of determination the center of the image as a center of gravity, after clipping the image wings at a certain level or at a certain radius, is closed into the case of z-tilt. Therefore, the processing program uses the expression (14). Note that the difference between the $W_{l,t}^g(0)$ and $W_{l,t}^z(0)$ is large enough and for a geometry of our device is 12%, and 17%. The difference between the $W_{l,t}^z(0)$ and the previously used formulas from [5] is less than 3% and 5% respectively.

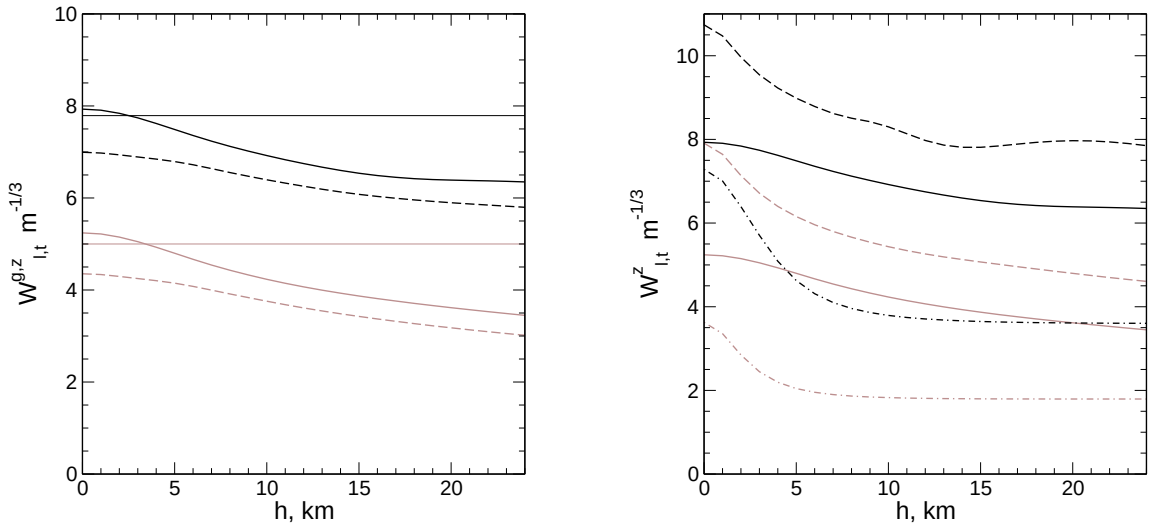


Figure 5: Left: Weight functions for our DIMM ($D = 0.09$, $B = 0.196$). Solid lines — $W^z_{l,t}(0)$,, dashed – $W^g_{l,t}(0)$, thin lines — the values computed by the formulas of [5]. Right: weighting functions DIMM: solid curves — our device, dashed — DIMMA IAC: $D = 0.05$, $B = 0.20$, dash-dot curves — miniDIMM: $D = 0.05$, $B = 0.05$. Functions for longitudinal motion marked in black, for transversal — by gray

Thus, for the DIMM permanently being in use with device MASS, does not necessarily seek to ensure that the approximation of the near field was carried out as much as possible. This enables a fundamentally alter the geometry of the device. For example, DIMM may consist of two 5 cm aperture, located close to each other. The sensitivity of such a device falls roughly twice — for heights larger than 10 km, the instrument will operate in the far field, but the lens about 10 cm in diameter can use as the feeding optics.

## 5 Polychromatic effect in differential motion

As already noted, the differential motion cease to be achromatic when we go beyond the near field $D^2 \gg \lambda z$. The question of influence polyhromatic radiation was studied in [13], however, from a practical point of view, the approach shown in [12] for the case of polychromatic scintillation is preferable.

The magnitude of the differential displacement of star images in DIMM geometry $\alpha(\lambda)$ depends on the wavelength if take into account the propagation effect. Considering a thin turbulent layer at an altitude of $z$ we can write:

$$\alpha(\lambda) = \int \tilde{\phi}(\vec{f},\lambda)\tilde{\psi}(\vec{f},\lambda)\cos(\pi\lambda z f^2)\mathrm{d}\vec{f}, \tag{17}$$

where aperture filter is included in DIMM spectral filter $\tilde{\psi}(\vec{f},\lambda)$, $\tilde{\phi}(\vec{f},\lambda)$ — phase fluctuation spatial spectrum. The integration is over all two-dimensional spatial frequencies $\vec{f}$. When

differential motion is measured in some spectral band, the integration over the wavelength must be performed:

$$\alpha = \int \alpha(\lambda) A(\lambda) \mathrm{d}\lambda, \tag{18}$$

where $A(\lambda)$ — the normalized spectral characteristics of radiation.

Hence, knowing that $\langle\alpha\rangle \equiv 0$, we can determine the variance $\sigma^2 = \langle\alpha^2\rangle$ of differential motion

$$\sigma^2 = \iint \langle\alpha(\lambda_1)\alpha(\lambda_2)\rangle A(\lambda_1) A(\lambda_2) \mathrm{d}\lambda_1 \mathrm{d}\lambda_2 \tag{19}$$

The expression for the covariance $\langle\alpha(\lambda_1)\alpha(\lambda_2)\rangle$ is obtained from (17):

$$\langle\alpha(\lambda_1)\alpha(\lambda_2)\rangle = \iint \langle\tilde{\phi}(\vec{f_1}, \lambda_1)\tilde{\phi}^*(\vec{f_2}, \lambda_2)\rangle \tilde{\psi}(\vec{f_1}, \lambda_1)\tilde{\psi}^*(\vec{f_2}, \lambda_2) \cos(\pi\lambda_1 z f_1^2) \cos(\pi\lambda_2 z f_2^2) \mathrm{d}\vec{f_1} \mathrm{d}\vec{f_2} \tag{20}$$

We use the expression (10) from the work [12]:

$$\langle\tilde{\phi}(\vec{f_1}, \lambda_1)\tilde{\phi}^*(\vec{f_2}, \lambda_2)\rangle = F_\phi(\vec{f_1})\delta(|\vec{f_1} - \vec{f_2}|) = \frac{4\pi^2}{\lambda_1\lambda_2} F_l(\vec{f_1})\delta(|\vec{f_1} - \vec{f_2}|), \tag{21}$$

what allows to reduce the double integral to a single, and determining achromatic spectral filter $\Phi_d(\vec{f_1}, \vec{f_2}) = \frac{4\pi^2}{\lambda_1\lambda_2}\tilde{\psi}(\vec{f_1}, \lambda_1)\tilde{\psi}^*(\vec{f_2}, \lambda_2)$, we obtain (20) as follows:

$$\langle\alpha(\lambda_1)\alpha(\lambda_2)\rangle = \int F_l(\vec{f})\Phi_d(\vec{f}) \cos(\pi\lambda_1 z f^2) \cos(\pi\lambda_2 z f^2) \mathrm{d}\vec{f} \tag{22}$$

Thus, we clearly selected the dependence on $\lambda$. Now, the covariance can be substituted into the expression (19), reversing the order of integration and denoting

$$S_A(\vec{f}, z) = \iint A(\lambda_1)A(\lambda_2) \cos(\pi\lambda_1 z f^2) \cos(\pi\lambda_2 z f^2) \mathrm{d}\lambda_1 \mathrm{d}\lambda_2 = \left[\int A(\lambda) \cos(\pi\lambda z f^2) \mathrm{d}\lambda\right]^2. \tag{23}$$

The result is the following expression for the variance of differential motion:

$$\sigma^2 = \int F_l(\vec{f})\, \Phi_d(\vec{f})\, S_A(\vec{f}, z) \mathrm{d}\vec{f} \tag{24}$$

The function $S_A(\vec{f}, z)$ is a square of the real part of the Fourier transform of the distribution of energy in the radiation spectrum [12] and depends only on the modulus of frequency:

$$S_A(f, z) = [\tilde{A}(zf^2/2)]^2. \tag{25}$$

Unlike the case of scintillation the Fourier transform is taken from the distribution itself rather than distribution divided by $\lambda$. The reason is that the motion in the near field doesn't depend on wavelength, but the scintillation always depends on $\lambda$.

The expression (24) differs from the monochrome case only in that the usual Fresnel filter $\cos^2(\pi\lambda z f^2)$ is replaced by polychromatic filter $S_A(zf^2/2)$. Therefore, the results of previous section can be generalized to a wide spectral band of the detected light. Simply replace the filter in the expressions (13) and (14). Calculated for our device polychromatic Fresnel filter is shown in Fig. 6 on the left.

Example of normalized weighting function $W(z)$ for our DIMM is shown in Fig. 6 on right. It is seen that the difference from the monochromatic case is not so great. This is due to the fact that the wide band effect affects primarily at high spatial frequencies, and DIMM is sensitive to relatively low frequencies.

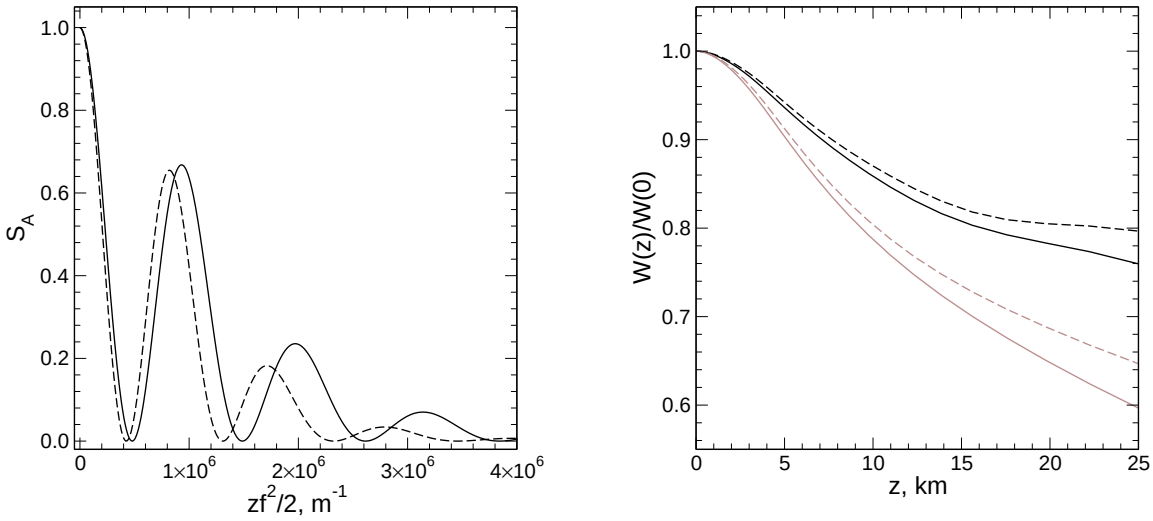


Figure 6: Left: polychromatic Fresnel filter for EC650 CCD camera and star of spectral class A0 V (solid line) and K0 III (dashed line). Right: weighting functions of our DIMM for polychromatic case (solid curves) and for monochrome light corresponding to the effective wavelength (dashed) of spectral class A0 V. Longitudinal motion is black, transversal one is gray

## 6 Finite exposure effect

Understanding that wind shifts the turbulence at distance comparable to the size of the DIMM aperture within a typical camera exposure of 0.01 s, gave rise to the theory [2] and experimental [14] studies the effect of exposure length to the measured. power of differential motion. The significance of this effect led to the appearance of methods of correction involving or not an additional data.

In practice, measurements with the DIMM instrument and its processing is most often used method of interlacing exposures (see, eg, [4]). The essence of this method lies in the alternation exposures with the usual length and doubled, for example, 5 and 10 ms. Next, for these series the image quality is separately calculated and the resulting seeing is obtained as some combination of them.

When working with high-speed cameras such method does not apply, because you can not change the exposure without stopping the video stream. Therefore, the program *dimm* when processing frames calculates additional correlation between adjacent measurements of the images. The theoretical basis of the correction using the correlation described below.

Estimation of the effect can be obtained by multiplying the temporal power spectrum of the motion on the spectral filter of signal averaging during the exposure $\tau$. In the paper [2] the spatial averaging over the coordinate x (we recall that the x-axis is directed along the wind) in a rectangular window with a width equal to the value of wind shear $w\tau$ is used:

$$\sigma_1^2(w\tau) = \iint_{-\infty}^{\infty} \mathrm{d}f_x\,\mathrm{d}f_y\,F_d(f_x,f_y)\,\mathrm{sinc}^2(f_x w\tau), \tag{26}$$

where the factor $\mathrm{sinc}^2(f_x w\tau)$ — the spectral filter is one that meets such averaging. Natu-

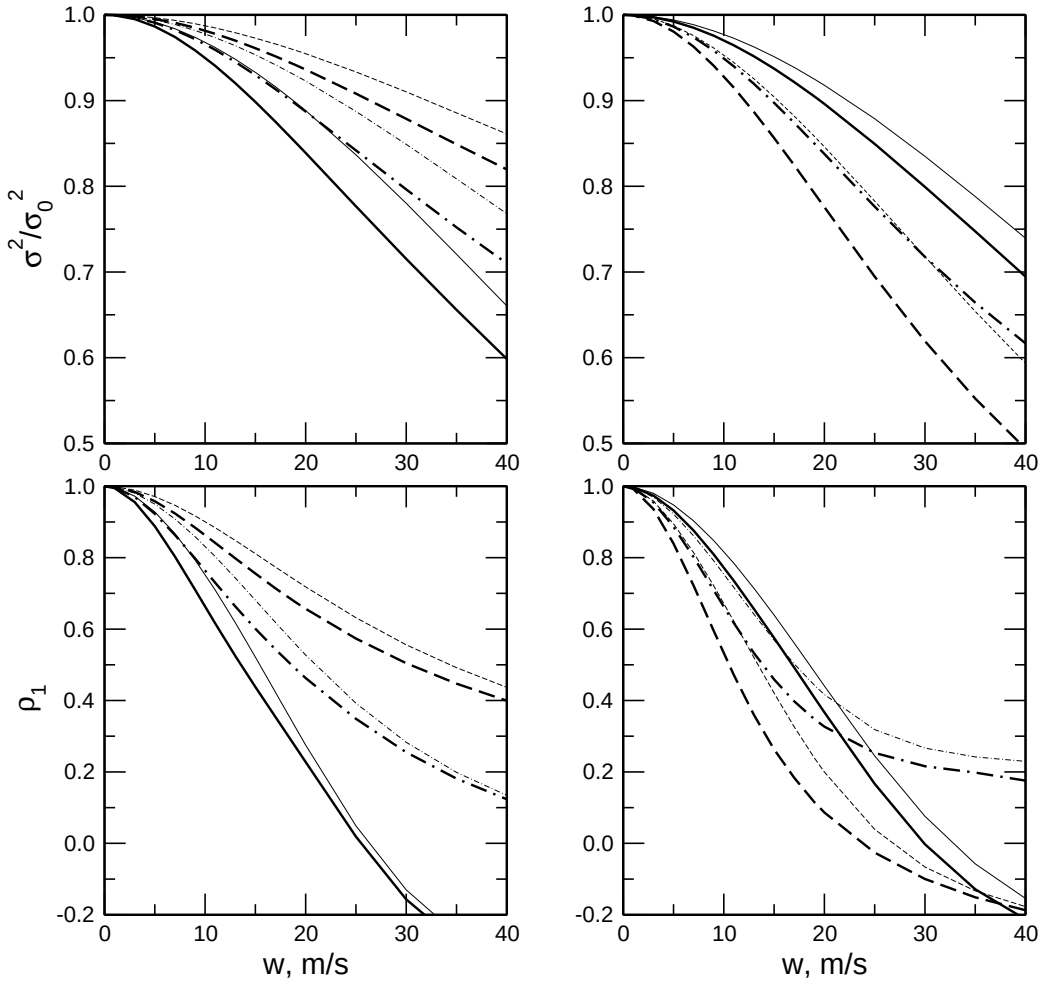


Figure 7: Upper row: the relative drop in variance $\sigma^2(w)$ of the differential motion, depending on wind speed. Bottom row: the correlation coefficient of nearby exposures $\rho_1$. Left column: longitudinal motion, right column: transversal motion. The solid curves denotes the case of wind along the base, the dashed curves — wind across the base, dashed-dotted — under angle 45°. Thick curves — wave propagation is not taken into account (low turbulence), thin curves — propagation from a height 16 kilometers (high turbulence). The curves are calculated for exposure 4 ms and frames period 5 ms

rally, the result depends on the orientation of the DIMM base on the wind and the measured components of motion.

Similarly, when averaged over two successive exposures $\tau$ with period $\tau_p$ ($\tau_p \geq \tau$) the motion variance $\sigma_2^2(w\tau, \tau_p)$ looks like:

$$\sigma_2^2(w\tau, \tau_p) = \iint_{-\infty}^{\infty} \mathrm{d}f_x \, \mathrm{d}f_y \, F_d(f_x, f_y) \, \mathrm{sinc}^2(f_x w\tau) \, \cos^2(\pi f_x w\tau_p), \tag{27}$$

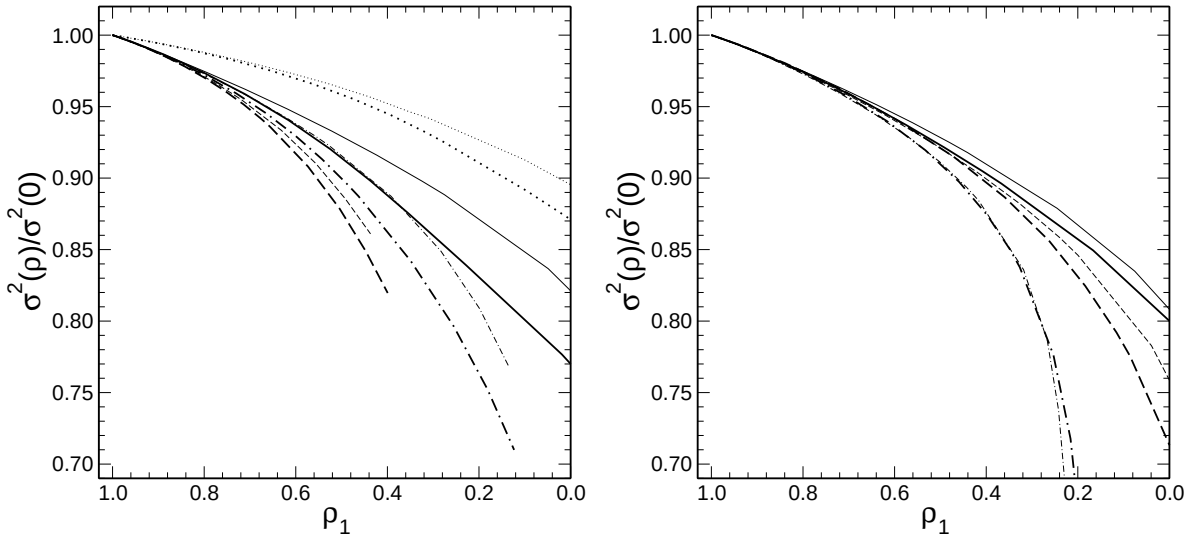


Figure 8: Dependence of the variance on the correlation coefficient $\rho_1$. On left — for longitudinal motion, ot right — for transversal one. The curves marked as in Fig. 7. For comparison, in the left plot behavior for the longitudinal wind and exposure 2.5 ms are shown by dotted curves

where $\mathrm{sinc}^2(f_x w\tau)\ \cos^2(\pi f_x w\tau_p)$ is the filter corresponding to such averaging.

The coefficient of correlation of positions in proximate image frames $\rho_1$ is expressed through these quantities as follows:

$$\rho_1 = \frac{2\sigma_2^2(w\tau, \tau_p)}{\sigma_1^2(w\tau)} - 1 \tag{28}$$

In Fig. 7 the calculated dependence $\sigma^2(w\tau)/\sigma^2(0)$ and the correlation coefficient $\rho_1$ on the wind speed for different situations are shown, performed for our DIMM instrument and camera settings: $\tau = 4$ ms and $\tau_p = 5$ ms.

The graphs show that the transversal more susceptible to the effect of discussion and with the wind speed, reaching to 40 m/s in the tropopause, only 50 – 70% power is measured, even at fairly short exposure. Given the propagation somewhat reduces the effect, since it weakens the high-frequency part of the spectrum. Different wind directions bring additional uncertainty about 2 times into fraction of power loss.

The behavior of quantity $\rho_1$ is also strongly dependent on the wind direction in the turbulent layer. However, we note that the extreme situations: the wind is strictly along the base or severely across virtually not implemented due to random variations of wind direction. Rated characteristic value of these variations and considerations of symmetry of the spatial spectrum of differential motion leads to the fact that the real uncertainty will be considerably less.

Moreover, the dependence on the direction for the measured power $\sigma^2(w\tau)$ is partially compensated by syn-phase dependence of the correlation coefficient and the dependence of $\sigma^2(w\tau)$ on $\rho_1$, shown in Fig. 8, looks more determinately, for the exception is the case of transversal motion at a wind angle of 45°. These relations will be used for calculating of the correction by finite exposure time

# 7 Correction of the differential motion power

In the works [2, 14] the correction was evaluated on the basis of model assumptions about the profiles of $C_n^2(h)$ and of the wind speed $w(h)$. The method of interlaced exposures as well as the method of measured correlation are developed for correction, independent of the model assumptions. The problem is that the dependences shown in Fig. 8, are implemented within separate thin layer.

Let us show that, at least in the case of linear approximation, the correction to zero exposure is possible for measured values $\tilde{\sigma}^2$ and $\rho_1$. Conventionally, we denote the motion power caused by a layer at a height of $h$ as $\tilde{\sigma}^2(h)$ and the covariance $\tilde{\sigma}^2(h)\rho_1(h)$. Since the covariance as well as dispersion, are formed in complete independence of phase distortions in the different layers (the main paradigm of weak perturbations), then the totals can be written:

$$\tilde{\sigma}^2 = \int \tilde{\sigma}^2(h)\,\mathrm{d}h, \qquad \tilde{\sigma}^2\rho_1 = \int \tilde{\sigma}^2(h)\rho_1(h)\,\mathrm{d}h \tag{29}$$

The true (at zero exposure) power $\sigma^2$ will be presented as

$$\sigma^2 = \int \sigma^2(h)\,\mathrm{d}h = \int \tilde{\sigma}^2(h)\cdot f(\rho_1(h))\,\mathrm{d}h, \tag{30}$$

where $f(\rho_1(h))$ — corrective function, whose argument is correlation coefficient in the layer. If this function is described by a linear law $a_0 + a_1\rho_1$ then we can write (30) in the form:

$$\sigma^2 = \int \tilde{\sigma}^2(h)(a_0 + a_1\rho_1(h))\,\mathrm{d}h = a_0\int \tilde{\sigma}^2(h)\,\mathrm{d}h + a_1\int \tilde{\sigma}^2(h)\rho_1(h)\,\mathrm{d}h = a_0\tilde{\sigma}^2 + a_1\tilde{\sigma}^2\rho_1. \tag{31}$$

More complex corrective function (which more precisely describes needed relationship) does not provide additivity and, therefore, in general, may give worse results. These same considerations apply to the method of interlaced exposures, that is, only the use of linear correction ensures its independence on the altitude turbulence distribution.

It should be borne in mind that Fig. 8 shows the behavior of $\tilde{\sigma}^2(\rho_1)/\sigma^2$ while the family of the corrective functions is an inverse relationship: $\sigma^2/\tilde{\sigma}^2(\rho_1)$.

To find the most probable linear approximation, the coefficients $\rho_1$, obtained in the measurements of 2007 – 2009 on top of Shatdzhatmaz, have been investigated. In Fig. 9, left, the cumulative distributions constructed by minute values are shows. Median of correlation coefficient are 0.85 for both components of the differential motion. The reliability of the curves is confirmed by the values of relative errors of $\rho_1$ constituting an average of 0.03.

The same figure on the right shows the medians of $\rho_1$ as function of the surface wind speed. It is seen that even in the absence of surface wind, measured dependences lies lower than estimated ones due to that in the free atmosphere wind is always present.

From the graphs presented in Fig. 8 implies that for 50% of our data, the needed correction is less than 2% (or about 1% in seeing $\beta$). For 90% of whole data correction is less than 5%. Nevertheless, using the differential distribution of the observed $\rho_1$ as weights, we have built corrective dependence as

$$\sigma^2 = \tilde{\sigma}^2\left(1 + 0.15(1-\rho_1)\right). \tag{32}$$

According to this formula for the marginal cases $\rho_1 < 0.5$ the correction is about 8% of the OT intensity.

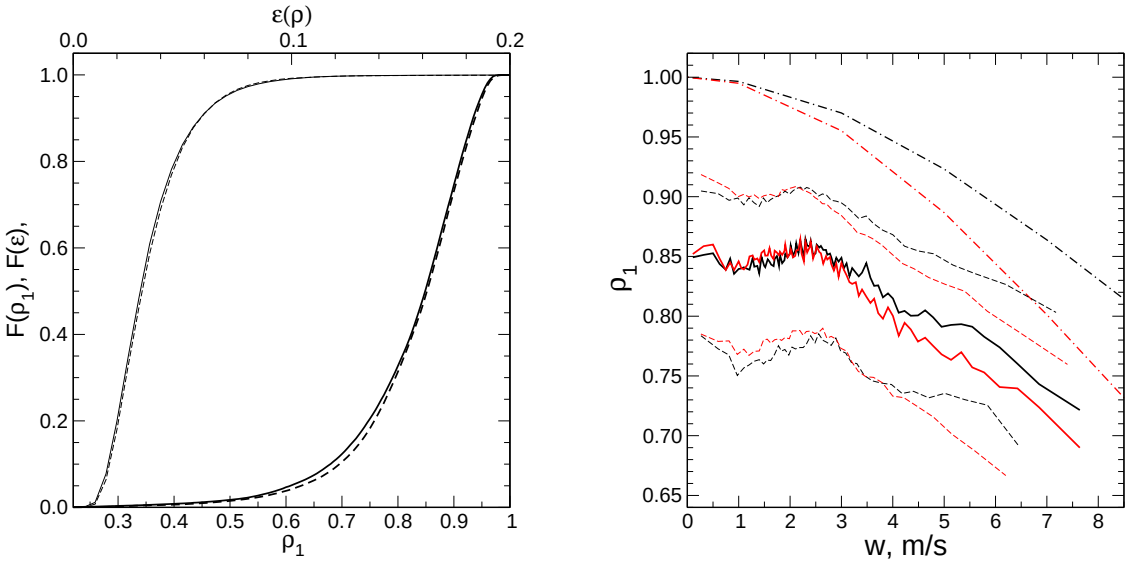


Figure 9: Left: cumulative distributions of the observed correlation $\rho_1$ (bold curves). Solid lines denote longitudinal motion, dashed lines — transversal motion. The thin lines are presented the distribution of the relative errors $\epsilon$ of $\rho_1$ within 1 min accumulation (upper scale). Right: the dependence of the median values of the measured $\rho_1$ on the wind speed for the longitudinal (black line) and transversal components (red). Thin dashed lines indicate 25 and 75 % quartiles. The dash-dotted curves are calculated dependences for the wind 45°.

Preliminary analysis of measurements with our DIMM device showed that exposure 4 ms is too long for the brightest stars due to signal saturation in the image center.. Therefore, from the December 2009 the exposure was reduced to 2.5 ms. In Fig. 8 on left, dashed line marks the relation for such exposure. It is evident that the magnitude of the required correction is reduced almost by half.

## References


[1] Fried D.L., JOSA, 55, p. 1427, 1965

[2] Martin H.M., PASP, V. 99, p. 1360, 1987

[3] Fried D.L., Radio Science, 10, p. 71, 1975

[4] Tokovinin A., PASP, **114**, 1156, 2002

[5] Sarazin M. Roddier F., Astron. Astrophys., 227, p.294, 1990

[6] Thomas-Osip J., Prieto G., Johns M., Phillips M.,Proceedings of the SPIE, V. 7012, pp. 70121U-70121U-12, 2008

[7] Tatarskii V.I., 1961, Wave Propagation in a Turbulent Medium. Dover Press, New York

[8] Tokovinin A., Baumont S., Vasquez J., MNRAS, V. 340, Issue 1, pp. 52-58, 2003

[9] Tokovinin A., Kornilov V., MNRAS, **381**, 1179, 2007

[10] Tokovinin A., Kornilov V., in ASP Conference Proceedings, V. 266. Edited by J. Vernin, Z. Benkhaldoun, and C. Muñoz-Tuñón, p.104, 2002

[11] Kornilov V., Tokovinin A., Voziakova O., Zaitsev A., Shatsky N., Potanin S., Sarazin M., Proc. SPIE, V. 4839, p. 837, 2003

[12] Tokovinin A., JOSA(A), 2003, **20**, 686, 2003

[13] Berdja A., Borgnino J., Irbah A., Journal of Optics A: Pure and Applied Optics, V. 8, Issue 3, p. 244, 2006

[14] Soules D.B., Drexler J.J., Draayer B.F., et al, PASP, **108**, 817, 1996